ISSN 2070-0482, Mathematical Models and Computer Simulations, 2022, Vol. 14, No. 4, pp. 578–589. © Pleiades Publishing, Ltd., 2022.
Russian Text © The Author(s), 2021, published in Matematicheskoe Modelirovanie, 2021, Vol. 33, No. 12, pp. 49–66.

Entropic Regularization of the Discontinuous Galerkin Method in Conservative Variables for Two-Dimensional Euler Equations

M. D. Bragin[a, *], Y. A. Kriksin[a, **], and V. F. Tishkin[a, *]**

[a] *Keldysh Institute of Applied Mathematics, Russian Academy of Sciences, Moscow, Russia*

**e-mail: michael@bragin.cc*

***e-mail: kriksin@imamod.ru*

****e-mail: v.f.tishkin@mail.ru*

Received September 28, 2021; revised September 28, 2021; accepted November 8, 2021

Abstract—An entropic regularization of the conservative stable discontinuous Galerkin method (DGM) in conservative variables for two-dimensional Euler equations is constructed based on a special slope limiter. This limiter ensures the fulfillment of two-dimensional analogs of the monotonicity conditions and a discrete analog of the entropic inequality. The developed method was tested on two-dimensional model gas-dynamic problems.

Keywords: Euler equations, discontinuous Galerkin method, conservation laws, slope limiter, entropic inequality

DOI: 10.1134/S2070048222040056

1. INTRODUCTION

One of the promising areas of research in the development of numerical methods for solving gas-hydrodynamic problems is the creation of algorithms that are conservative and entropy stable [1–12]. Many different versions of entropically stable schemes have been proposed; however, research in this area is still far from complete.

Among the multitude of numerical methods used in the designated area, the discontinuous Galerkin method (DGM) should be singled out [13–19], which, on the one hand, is characterized by a compact stencil, and, on the other hand, by the potentially highly accurate finite element (FE) approximations. Various modifications of the DGM have been proposed that are conservative and possess the property of entropic stability [13, 20–25]. Nevertheless, there is still a need to further improve the entropically stable versions of the DGM in order to improve the quality of numerical solutions.

Initially, we proposed a variational method for the entropic regularization of the DGM, in which the values of the DGM coefficients are determined as a solution to some variational problem for the conditional minimum [20] with a convex constraint that ensures the fulfillment of the entropic inequality. However, it was soon discovered that the formal fulfillment of the entropic stability condition alone, which consists in the nonnegative production of entropy, is insufficient for the numerical stability of the algorithm [21]. Further, it was found that to ensure the computational stability of the algorithm, some degree of monotonicity of FE approximations is necessary. As a result, the set of constraints in the corresponding variational problem was supplemented by a system of linear inequalities expressing the monotonicity of FE approximations [22]. As a result of this modification, a computationally stable version of the entropically regularized DGM was obtained. When solving problems with two or more spatial variables, for example, multidimensional problems of gas dynamics, there is a need for effective generalizations of the concept of monotonicity. One of the possible approaches was proposed for the DGM in nonconservative variables in the case of the Euler equations [23–25]. In this paper, we construct an entropically stable DGM for the Euler equations in traditional conservative variables using the generalized monotonicity conditions similar to those used in [25]. The need to build a version of the DGM in conservative variables is due to two circumstances. First, conservative variables are traditionally used in numerical methods for problems in continuum mechanics. The study would be incomplete if we restricted ourselves to the case of nonconservative variables, which is not typical. Second, on the same grid, the algorithm in conservative variables

turns out to be more computationally efficient. The computational cost of the version in conservative variables for the same problems turns out to be lower by factors of 2 to 3 than the version in nonconservative variables. At the same time, the accuracy of the approximate solution on the selected test problems remains approximately the same.

The material of the work is presented in the following sequence. Section 2 consists of the problem statement; Section 3 derives the DGM equations in conservative variables *density*, *pulse density*, and *total gas energy*; in Section 4, the leading coefficients of FE approximations are limited based on the monotonicity condition generalized to the case of two spatial variables and the entropic stability condition; and in Section 5, the numerical results are discussed.

2. PROBLEM STATEMENT

We consider a system of Euler equations describing two-dimensional gas dynamics in dimensionless variables, for which we set an initial-boundary value problem in a rectangular domain Π:

$$\frac{\partial \mathbf{U}}{\partial t} + \frac{\partial \mathbf{F}_1(\mathbf{U})}{\partial x_1} + \frac{\partial \mathbf{F}_2(\mathbf{U})}{\partial x_2} = 0, \quad \mathbf{U}(\mathbf{x},0) = \mathbf{U}_0(\mathbf{x}), \\ \mathbf{x} = (x_1, x_2) \in \Pi = (a_1, b_1) \times (a_2, b_2), \quad t > 0, \tag{1}$$

where $\mathbf{U}(x,t) = (U^{(1)}, U^{(2)}, U^{(3)}, U^{(4)})^{\mathrm{T}}$ and $\mathbf{F}_j(\mathbf{U}) = (F_j^{(1)}, F_j^{(2)}, F_j^{(3)}, F_j^{(4)})^{\mathrm{T}}$ are column vectors of conservative variables and fluxes in the direction of axis Ox_j ($j = 1,2$), respectively. Conditions at the boundary $\partial\Pi$ of rectangle Π are given by ghost cells that are adjacent to the boundary $\partial\Pi$ outside (the boundary conditions are specified in Section 5). The ideal gas equation of state

$$p = (\gamma - 1)\rho\varepsilon, \quad \gamma = c_P/c_V \tag{2}$$

closes the system of equations (1). In Eqs. (1) and (2), the following notations are used: p is pressure, ρ is density, ε is specific internal energy, $\gamma = 1.4$ is the adiabatic index, and c_P and c_V are the heat capacities of an ideal gas at constant pressure and constant volume, respectively. Taking into account the equation of state (2), for the momentum density and total energy density, respectively, the following designations are used:

$$\mathbf{I} = (I_1, I_2), \quad I_j = \rho u_j, \quad E = p/(\gamma - 1) + (I_1^2 + I_2^2)/(2\rho), \tag{3}$$

where $\mathbf{u} = (u_1, u_2)$ is the velocity vector. Taking into account (3), the explicit expressions for the column vector of conservative variables and the column vector of fluxes, respectively, take the form

$$\mathbf{U} = \begin{pmatrix} \rho \\ I_1 \\ I_2 \\ E \end{pmatrix}, \quad \mathbf{F}_j(\mathbf{U}) = \begin{pmatrix} I_j \\ \rho^{-1} I_1 I_j + p\delta_{1,j} \\ \rho^{-1} I_2 I_j + p\delta_{2,j} \\ (E + p)\rho^{-1} I_j \end{pmatrix}, \tag{4}$$

where δ_{ij} is the Kronecker symbol.

Satisfaction of the entropic inequality [26]

$$\iint\limits_{\Omega} [(\rho s)(t + \Delta t) - (\rho s)(t)] dx_1 dx_2 + \int\limits_{t}^{t+\Delta t} d\tau \oint\limits_{\partial\Omega} s(I_1\nu_1 + I_2\nu_2) d\sigma \geq 0 \tag{5}$$

in any subdomain $\Omega \subset \Pi$ with a fairly smooth boundary $\partial\Omega$ is an important prerequisite for a physically correct description of gas-dynamic processes, where $\boldsymbol{\nu} = (\nu_1, \nu_2)$ is the outer normal vector to $\partial\Omega$ and s is the entropy density

$$s = \ln p - \gamma \ln \rho. \tag{6}$$

The numerical solution of problem (1) is based on the entropically regularized DGM, a general description of which is given in [22–25]. In contrast to [25], here we construct the classical DGM in conservative variables ρ, I, and E. The proposed algorithm is characterized by the implementation of discrete analogs of conservation laws and a discrete analog of the entropic inequality in variables ρ, I, and E.

3. EQUATIONS FOR THE DGM COEFFICIENTS

In a closed rectangle $\overline{\Pi} = \Pi \cup \partial\Pi$, we define a Cartesian grid with nodes

$$\mathbf{x}_{mn} = (x_1^{(m)}, x_2^{(n)}) = (a_1 + mh_1, a_2 + nh_2), \quad m = 0,\ldots,M; \quad n = 0,\ldots,N, \tag{7}$$

$$h_1 = (b_1 - a_1)/M, \quad h_2 = (b_2 - a_2)/N. \tag{8}$$

Obviously, grid (7) is related to a set of computational cells $K_{mn} = (x_1^{(m-1)}, x_1^{(m)}) \times (x_2^{(n-1)}, x_2^{(n)})$. Each cell K_{mn} has four neighbors (on the sides) that are nearest to it: $K_{m-1,n}$, $K_{m,n-1}$, $K_{m+1,n}$, and $K_{m,n+1}$ with which it exchanges mass, momentum, energy, and entropy.

We introduce the local variables

$$z_j = 2h_j^{-1}(x_j - x_j^{(m-1)}) - 1, \quad j = 1,2 \tag{9}$$

in order to use them to write equations for the DGM coefficients in a single calculation cell K_{mn}. Local variables (9) take values in the interval $(-1, 1)$.

To construct an approximate solution within the computational cell K_{mn}, we will use the local polynomial basis related to this cell. Let us present an approximate solution of problem (1) $\mathbf{U}_h$ in cell K_{mn} as a linear function of local space variables

$$\mathbf{U}_h(z_1, z_2, t) = \mathbf{U}_0(t) + \mathbf{U}_1(t)z_1 + \mathbf{U}_2(t)z_2, \tag{10}$$

limited formally to the second order of approximation. Using the standard technique for deriving equations for the DGM coefficients [12, 17, 18], we arrive at a system of ordinary differential equations (SODE) with respect to the required coefficients $\mathbf{U}_0(t)$, $\mathbf{U}_1(t)$, and $\mathbf{U}_2(t)$

$$\begin{gathered}\frac{d\mathbf{U}_0(t)}{dt} = \mathbf{B}_0 = -h_1^{-1}h_2^{-1}\oint\limits_{\partial K}\sum_{l=1}^{2}\nu_l\mathbf{F}_l d\sigma,\\ \frac{d\mathbf{U}_j(t)}{dt} = \mathbf{B}_j = -3h_1^{-1}h_2^{-1}\left[\oint\limits_{\partial K}\sum_{l=1}^{2}\nu_l z_j\mathbf{F}_l d\sigma - \int\limits_K\sum_{l=1}^{2}\frac{\partial z_j}{\partial x_l}\mathbf{F}_l dx_1 dx_2\right],\\ j = 1,2.\end{gathered} \tag{11}$$

Recall that in Eqs. (11) in integrals over the boundary ∂K of cell K (indices m and n are omitted for brevity) ν_l denotes the component of the external normal to the boundary ∂K along the axis Ox_l, and $\mathbf{F}_l$ is the corresponding numerical Godunov flux. The right parts of Eqs. (11) are transformed to the following form:

$$\mathbf{B}_0 = -\frac{1}{2h_1}\int_{-1}^{1}[\mathbf{F}_1(1,z_2) - \mathbf{F}_1(-1,z_2)]dz_2 - \frac{1}{2h_2}\int_{-1}^{1}[\mathbf{F}_2(z_1,1) - \mathbf{F}_2(z_1,-1)]dz_1, \tag{12}$$

$$\begin{aligned}\mathbf{B}_1 = -\frac{3}{2h_1}\Bigg\{&\int_{-1}^{1}[\mathbf{F}_1(1,z_2) + \mathbf{F}_1(-1,z_2)]dz_2\\ &- \frac{h_1}{h_2}\int_{-1}^{1}[\mathbf{F}_2(z_1,1) - \mathbf{F}_2(z_1,-1)]z_1 dz_1 - \int_{-1}^{1}dz_1\int_{-1}^{1}dz_2\mathbf{F}_1(z_1,z_2,t)\Bigg\},\end{aligned} \tag{13}$$

$$\begin{aligned}\mathbf{B}_2 = -\frac{3}{2h_2}\Bigg\{&\int_{-1}^{1}[\mathbf{F}_2(z_1,1) + \mathbf{F}_2(z_1,-1)]dz_1\\ &- \frac{h_2}{h_1}\int_{-1}^{1}[\mathbf{F}_1(1,z_2) - \mathbf{F}_1(-1,z_2)]z_2 dz_2 - \int_{-1}^{1}dz_1\int_{-1}^{1}dz_2\mathbf{F}_2(z_1,z_2,t)\Bigg\},\end{aligned} \tag{14}$$

where the components of the numerical fluxes $\mathbf{F}_j$ are considered as complex functions of local coordinates (9):

$$\mathbf{F}_j = \mathbf{F}_j(z_1, z_2, t) = \mathbf{F}_j(\mathbf{U}(z_1, z_2, t)). \tag{15}$$

Note that any explicit time discretization of SODE (11), generally speaking, does not generate a computationally stable numerical algorithm for the approximate solution of the Euler equations (1). To obtain a stable numerical method, it is necessary to modify system (11) accordingly.

4. ENTROPIC REGULARIZATION OF THE SYSTEM OF EQUATIONS FOR DGM COEFFICIENTS

Let us construct an entropic regularization of fully discrete explicit schemes based on SODE (11). Since the explicit Runge–Kutta methods of high orders of accuracy consist of intermediate steps similar to the Euler scheme, we restrict ourselves to considering the simplest explicit first-order time integration method based on the Euler scheme.

As is known, the explicit numerical integration of SODEs for the DGM coefficients (11) in the case of gas-dynamic problems with strong shock waves turns out to be unstable, and these coefficients require correction [12, 16]. The method of numerical integration must satisfy, at each time step, the discrete analogs of the laws of conservation of mass, momentum, total energy, and entropic inequality. Let us pay attention to the fact that the first equation in Eqs. (11) $d\mathbf{U}_0(t)/dt = \mathbf{B}_0$ just describes the discrete analog of the laws of conservation of mass, momentum, and energy for a cell K_{mn} [20, 22] in continuous time. Approximation of this equation by the explicit Euler method with a time step τ

$$\mathbf{U}_0(t+\tau) = \mathbf{U}_0(t) + \tau\mathbf{B}_0(t) \tag{16}$$

retains the conservation property. Discrete analogs of the corresponding conservation laws for a cell K_{mn} hold in discrete time $t = 0, \tau, 2\tau, \ldots$. Therefore, the transition rule (16) of zero coefficients to the next time layer remains unchanged.

Due to the orthogonality of the system of functions in the form of a linear combination of which an approximate solution is sought in (10); the equations for the remaining DGM coefficients do not affect the conservation property. Correction (regularization) of other coefficients in order to ensure the stability of the algorithm is usually done by limiting them [12, 16]. As a result, after correction, the numerical scheme for the remaining coefficients takes the form

$$\mathbf{U}_j(t+\tau) = \mathbf{U}_j(t) + \tau\tilde{\mathbf{B}}_j(t), \quad j = 1, 2. \tag{17}$$

Thus, instead of the original SODE (11), some modified system is numerically integrated. In the case of entropic regularization, in addition to stability, it is required to ensure that, at each time step, the discrete analog of the entropic inequality (5) is satisfied for the cell K_{mn}.

In the variational approach [22], the values $\tilde{\mathbf{B}}_j$ ($j = 1, 2$) in (17) can be considered as a solution to the problem of determining the conditional minimum point of the quadratic function

$$\Phi(\tilde{\mathbf{B}}_1, \tilde{\mathbf{B}}_2) = \sum_{j=1}^{2} \left\| \tilde{\mathbf{B}}_j(t) - \mathbf{B}_j(t) \right\|^2 \tag{18}$$

on some convex constraint set including the entropic inequality, where $\|\cdot\|$ denotes some Euclidean norm.

Since the solution of the conditional minimum problem for function (18) in each finite element K_{mn} at each time step is very computationally expensive, in practice we have to resort to approximate methods for solving problem (18) and simplified approaches, for example, limiting the DGM coefficients [22].

Let us list the conditions that an entropically regularized DGM must satisfy.

(I) FE approximations (10) must satisfy at each time step some generalized monotonicity conditions that ensure the stability of the numerical algorithm.

(II) Some of the gas dynamic parameters, such as gas density ρ, pressure p, and total energy density E, have positive values in their physical sense. The algorithm must ensure that the indicated parameters are positive at each time step.

(III) In each finite element K_{mn} entropic inequality (5) must be satisfied at each time step.

Let us ensure the fulfillment of each of conditions I–III in the version of the DGM proposed here.

Let each cell K_{mn} be put into correspondence with a real number f_{mn}; i.e., $f = \{f_{mn}\}$ can be viewed as a piecewise constant function defined at every cell K_{mn}. In addition, we define a finite set of integer two-dimensional vectors (translations) $\Lambda = \{(\alpha,\beta)\}$. To each cell $K_{mn} \subset \overline{\Pi}$, we assign a nonnegative number

$$S^{\Lambda}_{mn}(f) = \min_{\alpha,\beta\in\Lambda} \left| f_{m+\alpha,n+\beta} - f_{mn} \right| \tag{19}$$

and in what follows, as a working set of translations, we choose the set

$$\Lambda = \{(1,0);(-1,0);(0,1);(0,-1)\}. \tag{20}$$

Let us also define the quantities

$$D_{mn}(f) = \frac{\delta}{2} S^{\Lambda}_{mn}(f), \quad D^{+}_{mn}(f) = \min\left(\frac{\delta}{2} S^{\Lambda}_{mn}(f), (1-\sigma) f_{mn}\right) \tag{21}$$

for some parameters $\delta \in (0,+\infty)$ and $\sigma \in (0,1)$ and the limiting function

$$\Delta(x, M) = \begin{cases} 1, & |x| \le M, \\ M^{-1}|x|, \end{cases} \qquad x \in (-\infty,\infty), \quad M \in (0,\infty). \tag{22}$$

For the DGM coefficients $\mathbf{U}_1$ and $\mathbf{U}_2$ in cell K_{mn}, let us construct a limitation procedure, the purpose of which is to obtain their values that satisfy requirements I–III formulated above.

Considering the DGM coefficients $\mathbf{U}_0(t+\tau)$ already known as a result of applying formula (17) and denoting the set of values of components l of these coefficients for all cells as $\{U_0^{(l)}(t+\tau)\}$, we calculate the quantities

$$M = \begin{cases} D^{+}_{mn}(\{U_0^{(l)}(t+\tau)\}), & l = 1,4; \\ D_{mn}(\{U_0^{(l)}(t+\tau)\}), & l = 2,3 \end{cases} \tag{23}$$

and

$$r = \left|U_1^{(l)}(t) + \tau B_1^{(l)}(t)\right| + \left|U_2^{(l)}(t) + \tau B_2^{(l)}(t)\right|. \tag{24}$$

Next, we determine the corresponding DGM coefficients using the limiting function (22)

$$U_j^{(l)}(t+\tau) = \Delta(r, M)[U_j^{(l)}(t) + \tau B_j^{(l)}(t)]. \tag{25}$$

According to (17), we obtain $\tilde{\mathbf{B}}_j = \tau^{-1}[\mathbf{U}_j(t+\tau) - \mathbf{U}_j(t)]$.

The generalized monotonicity conditions consist of applying the method for calculating the DGM coefficients $\mathbf{U}_1$ and $\mathbf{U}_2$ in accordance with (23)–(25). Note that, together with these conditions, the positiveness of the gas density ρ ($l = 1$) and total energy density E ($l = 4$) is also ensured due to the use of the special limiter D^{+}_{mn} defined in (21).

To ensure positive pressure p in cell K_{mn}, generally speaking, requires an additional constraint on the DGM coefficients $\mathbf{U}_1$ and $\mathbf{U}_2$ in addition to what has just been discussed. Hence, we introduce an auxiliary function

$$Q(\lambda) = \frac{1}{2} \frac{[U_0^{(2)} + \lambda(\left|U_1^{(2)}\right| + \left|U_2^{(2)}\right|)]^2 + [U_0^{(3)} + \lambda(\left|U_1^{(3)}\right| + \left|U_2^{(3)}\right|)]^2}{U_0^{(1)} - \lambda(\left|U_1^{(1)}\right| + \left|U_2^{(1)}\right|)}, \tag{26}$$

dominating the kinetic energy in the cell, and the function

$$P(\lambda) = (\gamma - 1)[U_0^{(4)} - \lambda(\left|U_1^{(4)}\right| + \left|U_2^{(4)}\right|) - Q(\lambda)], \tag{27}$$

which is a lower bound for the pressure p in it.

To ensure that the pressure is positive, we check the condition

$$P(1) - \sigma P(0) \ge 0, \tag{28}$$

where the value of parameter σ is the same as in (21), the DGM coefficients $\mathbf{U}_1$ and $\mathbf{U}_2$ are calculated in accordance with (23)–(25), and the value $P(0)$ is considered positive. If inequality (28) is satisfied, then the values of coefficients $\mathbf{U}_1$ and $\mathbf{U}_2$ are kept the same. Otherwise, the latter are limited by the rule $\mathbf{U}_j \to \lambda \mathbf{U}_j$, where $\lambda \in [0,1)$ is the root of the equation

$$P(\lambda) = (1 - \sigma)P(0). \tag{29}$$

In order to avoid the complication of the notation further, we will keep the old notation $\mathbf{U}_1$ and $\mathbf{U}_2$ for the new values of coefficients $\lambda\mathbf{U}_1$ and $\lambda\mathbf{U}_2$.

Finally, we will provide fulfillment in the cell K_{mn} of the entropic inequality (5) in the approximate solution (10). To do this, we consider the linear function of local coordinates

$$\mathbf{V}_\mu(z_1, z_2, t) = \mathbf{U}_0(t) + \mu(\mathbf{U}_1(t)z_1 + \mathbf{U}_2(t)z_2), \tag{30}$$

where parameter $\mu \in [0,1]$, and define the pressure function for it

$$p_\mu(z_1, z_2, t) = (\gamma - 1)\left[V_\mu^{(4)} - \frac{(V_\mu^{(2)})^2 + (V_\mu^{(3)})^2}{2V_\mu^{(1)}}\right] \tag{31}$$

and the entropy function

$$S(\mu, t) = \frac{h_1 h_2}{2}\int\limits_{-1}^{1} dz_1 \int\limits_{-1}^{1} dz_2 V_\mu^{(1)}(\ln p_\mu - \gamma \ln V_\mu^{(1)}). \tag{32}$$

The last term on the left side of (5), which is a flux term, is approximated in accordance with the Euler scheme (16)

$$\Phi_S(t) = \oint\limits_{\partial K} s(I_1\nu_1 + I_2\nu_2)d\sigma\big|_t \cong \frac{1}{\Delta t}\int\limits_t^{t+\Delta t} d\tau \oint\limits_{\partial K} s(I_1\nu_1 + I_2\nu_2)\,d\sigma. \tag{33}$$

The next approximation of the left side of inequality (5)

$$P_S(\mu) = S(\mu, t + \tau) - S(1, t) + \tau\Phi_S(t) \tag{34}$$

will be called the discrete analog of entropy production in cell $K = K_{mn}$. Next, we choose value $\mu \in [0,1]$ according to the rule

$$\mu = \begin{cases} 1, & P_S(1) \geq 0; \\ \mu^*, & P_S(\mu^*) = 0, \end{cases} \tag{35}$$

and we use expression (30) with the value (35) of the parameter μ as an approximate solution to (10) in cell K_{mn}.

5. RESULTS AND DISCUSSION

Let us check the DGM developed in Section 4 with an entropic slope limiter in conservative variables on the two-dimensional Riemann problems from [27]. Each of these problems is posed as follows: at $t = 0$ the computational domain $0 < x, y < 1$ ($a_1 = a_2 = 0$, $b_1 = b_2 = 1$) is divided into four equal squares (quarters), in each of which some constant density, pressure and velocity are specified (see Table 1). The gas is assumed to be diatomic, $\gamma = 1.4$. A symmetry condition is set on the boundary of the computational domain: $\partial\mathbf{U}/\partial n = 0$. It is required to determine the gas flow up to the time $t = t_{\max}$ inclusive.

Calculations using the regularized DGM will be performed on a grid of 200 × 200 cells with the following parameter values: $\delta = 2$ and $\sigma = 10^{-5}$ with the Courant number 0.2. The integrals are calculated using the Gauss method. In addition, we will make a comparison with the bicompact SDIRK3B4 scheme from [28]. This scheme uses locally one-dimensional splitting and the conservative monotonization method. On smooth solutions, the SDIRK3B4 scheme has the fourth order of approximation in space and the second order in time. The calculations according to the bicompact scheme were performed on the same grid of 200 × 200 cells, with the Courant number 0.8 and monotonization parameter $C_1 = 10$.

Table 1. Initial gas parameters and values t_{max} in two-dimensional Riemann problems

Problem		Left quadrant				Right quadrant				t_{max}
		p	ρ	u_1	u_2	p	ρ	u_1	u_2	
3	upper	0.3	0.5323	1.206	0	1.5	1.5	0	0	0.3
	lower	0.029	0.138	1.206	1.206	0.3	0.5323	0	1.206	
4	upper	0.35	0.5065	0.8939	0	1.1	1.1	0	0	0.25
	lower	1.1	1.1	0.8939	0.8939	0.35	0.5065	0	0.8939	
6	upper	1	2	0.75	0.5	1	1	0.75	−0.5	0.3
	lower	1	1	−0.75	0.5	1	3	−0.75	−0.5	
12	upper	1	1	0.7276	0	0.4	0.5313	0	0	0.25
	lower	1	0.8	0	0	1	1	0	0.7276	
15	upper	0.4	0.5197	−0.6259	−0.3	1	1	0.1	−0.3	0.2
	lower	0.4	0.8	0.1	−0.3	0.4	0.5313	0.1	0.4276	
17	upper	1	2	0	−0.3	1	1	0	−0.4	0.3
	lower	0.4	1.0625	0	0.2145	0.4	0.5197	0	−1.1259	

Problem 3. The lines of the initial discontinuities in this problem are shock wave fronts. In the process of their motion, three new shock waves arise. The latter limit the zone, in which the pressure is lower than the initial pressure in the upper right quarter of the computational domain. This difference in pressure causes a mass injection that has the shape of a mushroom in the density isoline pattern. Accordingly, the resolution of this smooth mushroom structure and seven shock waves is of interest.

Figure 1 shows at $t = 0.3$ entropy production rate P_s in the DGM and solutions (parameters p, ρ, u_1, u_2) for the DGM and the bicompact scheme. First of all, we note that the developed method of entropic regularization provides nonnegative entropy production in all cells, as was required. Both schemes resolve all shock waves equally well. However, the bicompact scheme resolves the aforementioned mushroom structure better, which is explained by its higher approximation orders (on smooth solutions).

Problem 4. Similarly to Problem 3, the initial discontinuities are shock waves. As they diverge, they create an area of increased pressure in the form of a lens bounded by two new shock waves. The shock wave propagation velocities in Problem 4 are higher than in Problem 3. In addition, the solution of Problem 4 does not contain structures of other types, which makes it possible to test the schemes on shock waves with greater clarity.

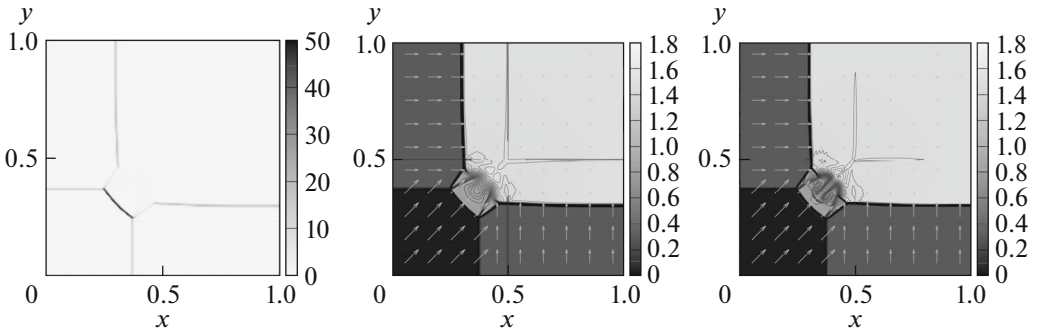

Fig. 1. Results in Problem 3, time $t = 0.3$. Left: plot of entropy production in the DGM. Center: flow pattern obtained by DGM. Color fill shows pressure, isolines show density (values from 0.16 to 1.71 with a step of 0.05), vectors show velocity (with a multiplier of 0.05). Right: flow pattern obtained by the bicompact scheme. All calculations were performed on a grid of 200 × 200 cells.

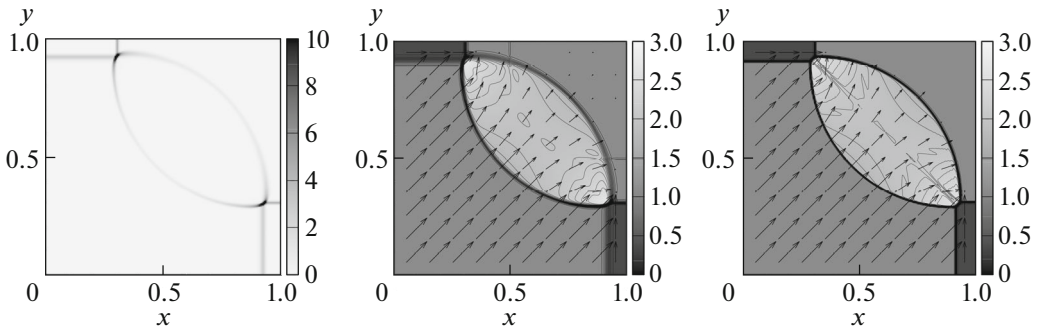

Fig. 2. Results in Problem 4, time $t = 0.25$. Left: plot of entropy production in the DGM. Center: flow pattern obtained by DGM. Color fill shows pressure, isolines show density (values from 0.52 to 1.92 with a step of 0.05), vectors show velocity (with a multiplier of 0.1). Right: flow pattern obtained by the bicompact scheme. All calculations were performed on a grid of 200 × 200 cells.

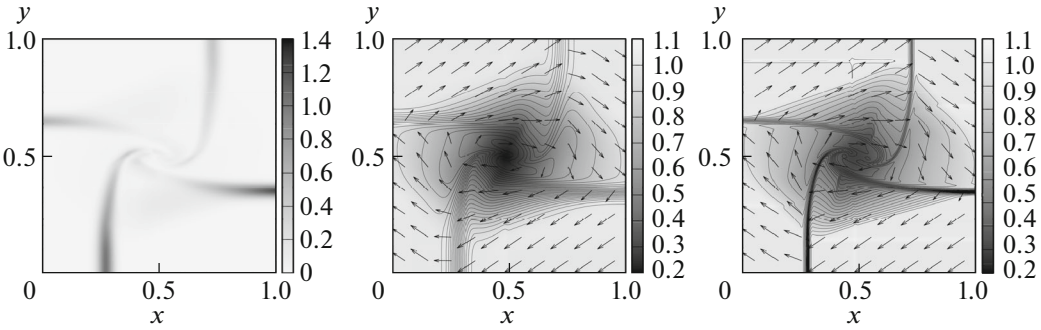

Fig. 3. Results in Problem 6, time $t = 0.3$. Left: plot of entropy production in the DGM. Center: flow pattern obtained by DGM. Color fill shows pressure, isolines show density (values from 0.25 to 3.05 with a step of 0.1), vectors show velocity (with a multiplier of 0.1). Right: flow pattern obtained by the bicompact scheme. All calculations were performed on a grid of 200 × 200 cells.

The flow patterns at $t = 0.25$, obtained by the DGM and the bicompact scheme, are shown in Fig. 2. It can be seen that the DGM smears the shock waves more strongly when compared with the results in Problem 3. Entropy production is nonnegative in all cells; it is maximum in shock waves. The bicompact scheme demonstrates the same spatial resolution as in the previous problem. Note that the solution calculated by the bicompact scheme contains small nonmonotonicities near the convergence points of the shock waves.

Problem 6. This problem tests the resolution of four moving contact discontinuities. In addition to them, the gas also has a diamond-shaped zone of moderate rarefaction.

From the visualizations of the flows at $t = 0.3$ in Fig. 3, we can conclude that the entropically regularized DGM resolves moving contact discontinuities on 16–20 cells. Excessive numerical dissipation also shows up in the entropy production plot. The bicompact scheme resolves contact discontinuities on 5 to 6 cells, which is typical for schemes of this class and order of accuracy. Nevertheless, the bicompact scheme allows a negative production of entropy on rarefaction waves, but it is small and amounts to $O(\tau^3)$ at $\tau \to 0$ [29].

Problem 12. The initial jumps in this problem are two shock waves and two stationary contact discontinuities. Moving away from the center of the computational domain, the shock waves leave behind a high-pressure zone bounded by two new shock waves. The fact that the solution of Problem 12 contains both shock waves and contact discontinuities (moreover, stationary) distinguishes it from Problems 3, 4, and 6 considered above.

Figure 4 shows at time $t = 0.25$ entropy production in the DGM and solutions calculated using the DGM and the bicompact scheme. As before, the new entropic regularization method excludes negative

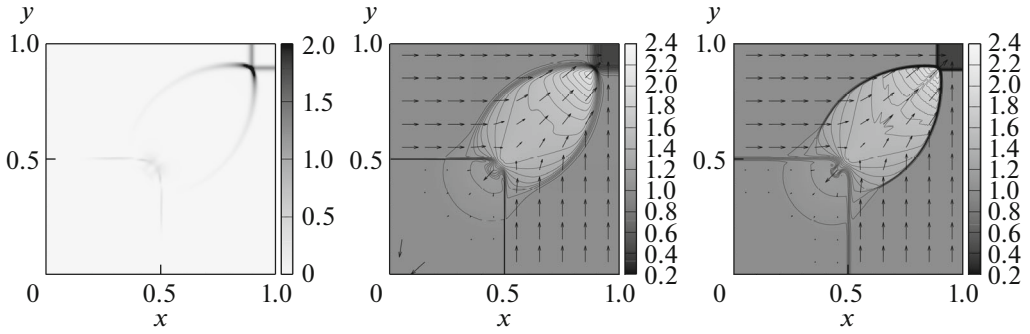

Fig. 4. Results in Problem 12, time $t = 0.25$. Left: plot of entropy production in the DGM. Center: flow pattern obtained by DGM. Color fill shows pressure, isolines show density (values from 0.54 to 1.7 with a step of 0.04), vectors show velocity (with a multiplier of 0.1). Right: flow pattern obtained by the bicompact scheme. All calculations were performed on a grid of 200 × 200 cells.

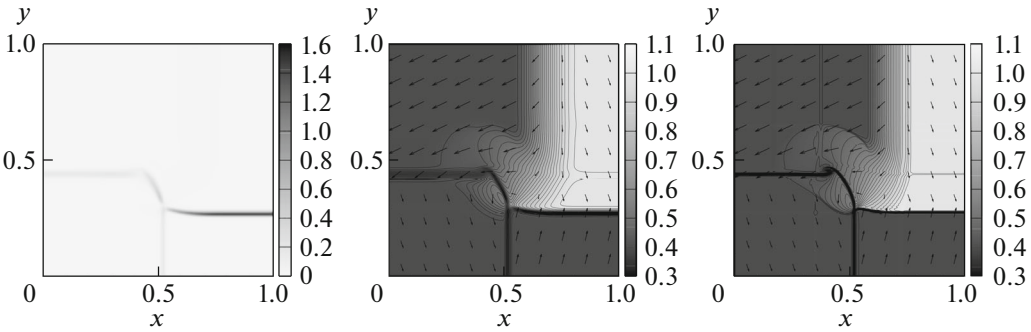

Fig. 5. Results in Problem 15, point in time $t = 0.2$. Left: plot of entropy production in the DGM. Center: flow pattern obtained by DGM. Color fill shows pressure, isolines show density (values from 0.43 to 0.99 with a step of 0.02), vectors show velocity (with a multiplier of 0.1). Right: flow pattern obtained by the bicompact scheme. All calculations were performed on a grid of 200 × 200 cells.

values P_s. Note that the DGM resolves stationary contact discontinuities on one cell, which is explained by the well-known property of the numerical Godunov flux. The bicompact scheme uses the global Lax–Friedrichs flux splitting, so its resolution of contact discontinuities does not depend on the velocities. The contact discontinuity is smeared by a bicompact scheme into 5 cells, as in Problem 6. As for the resolution of shock waves, it repeats that obtained in Problem 4.

Problem 15. At the initial moment of time, the quarters of the computational domain are separated by two moving contact discontinuities, the shock wave, and the discontinuity, which subsequently turns into a continuous rarefaction wave. As the gas moves, two small-amplitude shock waves additionally appear in it. A feature of this problem (relative to Problems 3, 4, 6, 12) is the presence of all three typical structures: a rarefaction wave, a contact discontinuity, and a shock wave.

Figure 5 shows at $t = 0.2$ the flow patterns calculated using the DGM and the bicompact scheme, as well as the graph P_s for the DGM. It can be seen that the second law of thermodynamics in the difference form holds in the regularized DGM without any violations. The width of the smearing of contact discontinuities in the DGM is proportional to their velocities, which corresponds to the results in Problems 6 and 12. The bicompact scheme still resolves these structures on five cells. The resolution of the primary shock wave in the DGM and in the bicompact scheme is almost the same.

Problem 17 is similar to Problem 15, the difference lies in the immobility of contact discontinuities in its initial condition. In the course of time, however, they begin to move in some of their parts.

The calculation results presented at $t = 0.3$ in Fig. 6 repeat what was obtained in the other problems. It is curious to note that the moving parts of contact discontinuities appear on the graph P_s due to their numerical dissipation.

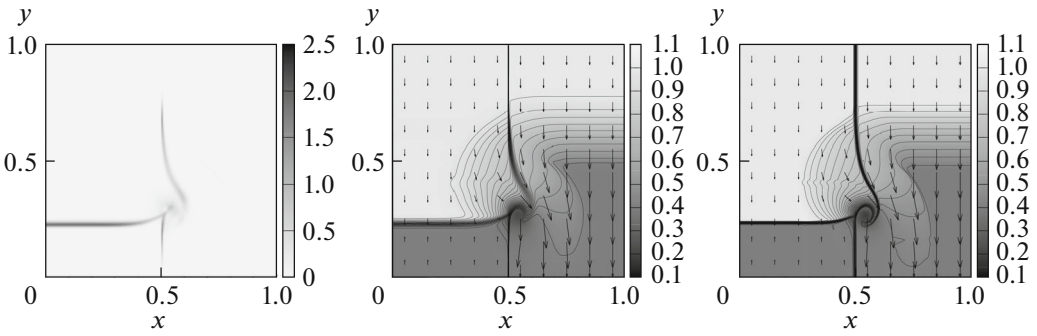

Fig. 6. Results in Problem 17, time $t = 0.3$. Left: plot of entropy production in the DGM. Center: flow pattern obtained by DGM. Color fill shows pressure, isolines show density (values from 0.54 to 1.99 with a step of 0.05), vectors show velocity (with a multiplier of 0.1). Right: flow pattern obtained by the bicompact scheme. All calculations were performed on a grid of 200 × 200 cells.

6. CONCLUSIONS

A new conservative entropically stable version of the discontinuous Galerkin method in conservative variables for the Euler equations with two space variables is proposed, which can be generalized in an obvious way to equations with three space variables. The advantage of the proposed method is nonnegativity of the entropy production.

A new conservative entropically stable version of the DGM was tested on problems from [27]. Its testing showed satisfactory results. Compared to the version of the DGM in nonconservative variables [25], the new algorithm turns out to be faster by factors of 2 to 3 in the same problems.

The high-order bicompact scheme has a better spatial resolution than the proposed version of the DGM, which is due to the higher order of accuracy of the bicompact scheme both in space and time. Further improvement of the quality of the numerical solution in the entropically stable version of the DGM is possible by increasing its approximation order and improving the procedure for correcting the leading coefficients of the DGM.

ACKNOWLEDGMENTS

The authors thank the Supercomputer Center of the Research Computing Center of Moscow State University and the Center for Information Technology of the University of Groningen (Netherlands) for the possibility of performing the calculations.

FUNDING

This study was supported by a grant from the Russian Science Foundation (project no. 21-11-00198).

CONFLICT OF INTEREST

The authors declare that they have no conflicts of interest.

REFERENCES

1. E. Tadmor, “Entropy stable schemes,” Handb. Numer. Anal. **17**, 467–493 (2016). https://doi.org/10.1016/bs.hna.2016.09.006
2. P. D. Lax, *Hyperbolic Systems of Conservation Laws and the Mathematical Theory of Shock Waves* (Soc. Ind. Appl. Math., Philadelphia, 1973). https://doi.org/10.1137/1.9781611970562
3. S. Osher, “Riemann solvers, the entropy condition, and difference approximations,” SIAM J. Numer. Anal. **21** (2), 217–235 (1984). https://doi.org/10.1137/0721016
4. F. Bouchut, Ch. Bourdarias, and B. Perthame, “A MUSCL method satisfying all the numerical entropy inequalities,” Math. Comput. **65** (216), 1439–1461 (1996). https://doi.org/10.1090/S0025-5718-96-00752-1

5. E. Tadmor, "Entropy stability theory for difference approximations of nonlinear conservation laws and related time-dependent problems," Acta Numer. **12**, 451–512 (2003).
https://doi.org/10.1017/S0962492902000156
6. F. Ismail and P. L. Roe, "Affordable, entropy-consistent Euler flux functions II: Entropy production at shocks," J. Comput. Phys. **228** (15), 5410–5436 (2009).
https://doi.org/10.1016/j.jcp.2009.04.021
7. P. Chandrashekar, "Kinetic energy preserving and entropy stable finite volume schemes for compressible Euler and Navier–Stokes equations," Commun. Comput. Phys. **14** (5), 1252–1286 (2013).
https://doi.org/10.4208/cicp.170712.010313a
8. U. S. Fjordholm, S. Mishra, and E. Tadmor, "Arbitrarily high-order accurate entropy stable essentially nonoscillatory schemes for systems of conservation laws," SIAM J. Numer. Anal. **50** (2), 544–573 (2012).
https://doi.org/10.1137/110836961
9. X. Cheng and Y. Nie, "A third-order entropy stable scheme for hyperbolic conservation laws," J. Hyperbolic Differ. Equat. **13** (1), 129–145 (2016).
https://doi.org/10.1142/S021989161650003X
10. V. V. Ostapenko, "Symmetric compact schemes with higher order conservative artificial viscosities," Comput. Math. Math. Phys. **7** (1), 980–999 (2002).
11. A. A. Zlotnik, "Entropy-conservative spatial discretization of the multidimensional quasi-gasdynamic system of equations," Comput. Math. Math. Phys. **57** (4), 706–725 (2017).
https://doi.org/10.1134/S0965542517020166
12. B. Cockburn, "An introduction to the Discontinuous Galerkin method for convection-dominated Problems," in *Advanced Numerical Approximation of Nonlinear Hyperbolic Equations*, Ed. by A. Quarteroni, Lecture Notes in Mathematics, Vol. 1697 (Springer, Berlin, 1997), pp. 150–268.
https://doi.org/10.1007/BFb0096353.
13. G. J. Gassner, A. R. Winters, and D. A. Kopriva, "A well balanced and entropy conservative discontinuous Galerkin spectral element method for the shallow water equations," Appl. Math. Comput. **272** (Part 2), 291–308 (2016).
https://doi.org/10.1016/j.amc.2015.07.014
14. N. Krais, A. Beck, T. Bolemann, H. Frank, D. Flad, G. Gassner, F. Hindenlang, M. Hoffmann, T. Kuhn, M. Sonntag, and C.-D. Munz, "FLEXI: A high order discontinuous Galerkin framework for hyperbolic-parabolic conservation laws," Comput. Math. Appl. **81**, 186–219 (2021).
https://doi.org/10.1016/j.camwa.2020.05.004
15. M. E. Ladonkina, O. A. Neklyudova, and V. F. Tishkin, "Application of averaging to smooth the solution in the DG method," KIAM Preprint No. 89 (Keldysh Inst. Appl. Math. RAS, Moscow, 2017) [in Russian].
https://doi.org/10.20948/prepr-2017-89.
16. M. E. Ladonkina, O. A. Neklyudova, and V. F. Tishkin, "Impact of different limiting functions on the order of solution obtained by RKDG," Math. Models Comput. Simul. **5** (4), 346–349 (2013).
https://doi.org/10.1134/S2070048213040091
17. M. E. Ladonkina and V. F. Tishkin, "Godunov method: a generalization using piecewise polynomial approximations," Differ. Equat. **51** (7), 895–903 (2015).
https://doi.org/10.1134/S0012266115070083
18. M. E. Ladonkina and V. F. Tishkin, "On Godunov-type methods of high order of accuracy," Dokl. Math. **91** (2), 189–192 (2015).
https://doi.org/10.1134/S1064562415020222
19. V. F. Tishkin, V. T. Zhukov, and E. E. Myshetskaya, "Justification of Godunov's scheme in the multidimensional case," Models Comput. Simul. **8** (5), 548–556 (2016).
https://doi.org/10.1134/S2070048216050124
20. Yu. A. Kriksin and V. F. Tishkin, "Entropic regularization of Discontinuous Galerkin method in one-dimensional problems of gas dynamics," KIAM Preprint No. 100 (Keldysh Inst. Appl. Math. RAS, Moscow, 2018) [in Russian].
https://doi.org/10.20948/prepr-2018-100.
21. M. D. Bragin, Yu. A. Kriksin, and V. F. Tishkin, "Verification of an entropic regularization method for discontinuous Galerkin schemes applied to hyperbolic equations," KIAM Preprint No. 18 (Keldysh Inst. Appl. Math. RAS, Moscow, 2019) [in Russian].
https://doi.org/10.20948/prepr-2019-18.
22. M. D. Bragin, Y. A. Kriksin, and V. F. Tishkin, "Discontinuous Galerkin method with an entropic slope limiter for Euler equations," Math. Models Comput. Simul. **12** (5), 824–833 (2020).
https://doi.org/10.1134/S2070048220050038
23. Yu. A. Kriksin and V. F. Tishkin, "Numerical solution of the Einfeldt problem based on the discontinuous Galerkin method," KIAM Preprint No. 90 (Keldysh Inst. Appl. Math. RAS, Moscow, 2019) [in Russian].
https://doi.org/10.20948/prepr-2019-90.

24. Yu. A. Kriksin and V. F. Tishkin, "Entropy-stable discontinuous Galerkin method for Euler equations using nonconservative variables," Math. Models Comput. Simul. **13** (3), 416–425 (2021). https://doi.org/10.1134/S2070048221030091
25. M. D. Bragin, Y. A. Kriksin, and V. F. Tishkin, "Entropy-stable discontinuous Galerkin method for two-dimensional Euler equations," Math. Models Comput. Simul. **13** (5), 897–906 (2021). https://doi.org/10.1134/S2070048221050069
26. S. K. Godunov, A. V. Zabrodin, M. Ya. Ivanov, A. N. Kraiko, and G. P. Prokopov, *Numerical Solution of Multidimensional Problems of Gas Dynamics* (Nauka, Moscow, 1976) [in Russian].
27. R. Liska and B. Wendroff, "Comparison of several difference schemes on 1D and 2D test problems for the Euler equations," SIAM J. Sci. Comput. **25** (3), 995–1017 (2003). https://doi.org/10.1137/S1064827502402120
28. M. D. Bragin and B.V. Rogov, "Conservative limiting method for high-order bicompact schemes as applied to systems of hyperbolic equations," Appl. Numer. Math. **151**, 229–245 (2020). https://doi.org/10.1016/j.apnum.2020.01.005
29. M. D. Bragin, "Entropy stability of bicompact schemes in gas dynamics problems," Math. Models Comput. Simul. **13** (4), 613–622 (2021). https://doi.org/10.1134/S2070048221040086